Journal of Sound and Vibration 329 (2010) 1137–1153

Contents lists available at ScienceDirect

Journal of Sound and Vibration

journal homepage: www.elsevier.com/locate/jsvi

Estimating the nonlinear resonant frequency of a single pile in nonlinear soil

Nicholas Andrew Alexander *,[1]

Department of Civil Engineering, University of Bristol, UK

ARTICLE INFO

Article history:
Received 18 February 2008
Received in revised form
21 October 2009
Accepted 21 October 2009
Handling Editor: M.P. Cartmell
Available online 13 November 2009

ABSTRACT

Analytical expressions are determined for the nonlinear resonant frequency (or natural frequency) of the fundamental lateral mode of a pile. A pile with a floating toe, with and without pile cap is considered in this paper. The influence of a nonlinear soil spring model that varies with depth and a nonlinear damping model that is strain amplitude dependent is considered. A non-dimensional equation of motion for the system dynamics is derived from an energy based formulation. This equation is a Duffing's type nonlinear differential system that has nonlinear damping. Harmonic balance with numerical continuation is employed to determine the nonlinear resonance curves of the system. Comparison with some experimental results is made.

1. Introduction

Climate change has resulted in a change in societal requirements for energy production. The need for reduced CO_2 emissions and the perceived threats to the supply of carbon based energy sources has resulted in a return to renewable energy. For example, there has been a huge increase in wind energy production. Vast wind farms have been constructed both on- and off-shore. The off-shore wind turbines use a range of different types of foundations that are dependant on site conditions. Use of large monopile foundations is not uncommon. Efficient design requires simple design rules as well as complex computational modelling. Nonlinear finite element modelling of time varying loading histories, such as earthquakes, is a complex undertaking for a design engineer. Validation of results obtained by such a process is vital. So simple design formulae are very useful in practice. Thus, there is a need to develop good approximations to the nonlinear resonant frequency of piles in both linear and nonlinear soils.

It is surprising that, in the literature, there is no exact analytic expression for the natural frequency of a single pile in elastic medium. In the linear case, and constant soil stiffness with depth, researchers [1–4] suggest various semi-analytical/empirical expressions based on a simple equivalent cantilever system. Ref. [1] provides a method for obtaining an analytically accurate equivalent stiffness and mass of the pile that is based on linear soil. For the case of nonlinear soil no such resonant frequency estimates are available.

This paper considers a single pile, with an additional lumped mass at its head. It is embedded in a nonlinear soil. The linear natural frequency is estimated and in addition the nonlinear resonant frequency is obtained. This is for the case of nonlinear soil behaviour.

This paper uses a soil springs analogy (after Winkler) to model the soil. Nonlinear P–y curves (where P is spring load per unit length and y is lateral pile deflection) are employed to determine the spring stiffness vs. compression of these springs.

* Tel.: +0117 928 8687.
E-mail addresses: nick.alexander@bristol.ac.uk, dralex7.nick@gmail.com.
[1] Senior Lecturer in Structural Engineering.

0022-460X/$ - see front matter © 2009 Elsevier Ltd. All rights reserved.
doi:10.1016/j.jsv.2009.10.026

Nomenclature[2]

a_i	harmonic balance coefficients
a_g	peak ground acceleration (PGA) $(L)(T)^{-2}$
A	ground acceleration amplitude
c, c_1, c_2	Rayleigh damping coefficient $(F)(T)(L)^{-2}$
C_1, C_2	linear and nonlinear damping coefficients
$\mathbf{D}$	dynamic matrix for linear modal analysis
D	pile diameter (L)
EI	pile flexural rigidity $(F)(L)^2$
F	forcing parameter
k_0	initial modulus of subgrade reaction $(F)(L)^{-3}$
k_{w1}	linear soil spring constants $(F)(L)^{-2}$
k_{w2}	nonlinear soil spring constant $(F)(L)^{-4}$
$\mathbf{K}$	stiffness matrix for linear modal analysis
K_1	linear stiffness coefficient of system
K_2	nonlinear stiffness coefficient of system
K_g	linear stiffness coefficient of near–far-field boundary
L	total pile length (L)
m_h	mass of at head of pile $(F)(T)^2(L)^{-1}$
m_p	mass per unit length of pile $(F)(T)^2(L)^{-2}$
m	mass per unit length of pile and near field soil layer $(F)(T)^2(L)^{-2}$
M	total system mass
$\mathbf{M}$	mass matrix for linear modal analysis
M_g	effective mass at near–far-field boundary
P	soil spring load per unit length $(F)(L)^{-1}$
p	soil spring load per unit area $(F)(L)^{-2}$
P_u	ultimate bearing capacity at depth z $(F)(L)^{-1}$
P_{ub}	ultimate bearing capacity at base (toe) of pile $(F)(L)^{-1}$
$\mathbf{q}_i$	solution vector of harmonic balance continuation.
R	Rayleigh dissipative function $(F)(T)^{-1}(L)$
s	frequency, dimensional $(\text{rad})(T)^{-1}$
t	time (T)
u	scaled ordinate w
u_g	scaled ordinate w_g
U	total potential energy $(F)(L)$
T	total kinetic energy $(F)(L)$
$w(t)$	temporal ordinate of y
$w_g(t)$	temporal ordinate of y_g
$\mathbf{w}_q, \mathbf{w}$	vectors of generalised coordinates, for linear modal analysis
y	relative lateral pile deflection (L)
y_g	displacements of the near–far field boundary (L)
y_p	limit of deflection for problem domain (L)
z	ordinate along the pile (L)
α	mass ratio
β_1	nonlinear to linear stiffness ratio of system
β_2	mass ratio of far-field effective mass to pile and near-field mass
β_3	stiffness ratio of near–far-field boundary to pile and near-field stiffness
ε	strain in soil springs
$\zeta_b D$	breadth (out of plane) soil layer (L)
$\zeta_w L$	effective, in-plane, width of near-field soil layer (L)
η_1	linear soil to pile stiffness parameter
η_2	nonlinear soil to pile stiffness parameter
$\boldsymbol{\theta}_1, \boldsymbol{\theta}_2$	vectors of shifted Legendre polynomials, for linear modal analysis
μ_1	linear damping ratio
μ_2	nonlinear damping ratio
μ_n	nonlinear to linear damping parameter ratio
$\mu_{\max}$	maximum ratio of critical damping at large soil strain
ξ	ordinate along pile
Π	Lagrangian for linear modal analysis $(F)(L)$
ρ_s	density of near-field soil layer $(F)(T)^2(L)^{-4}$
τ	scaled time
$\phi(\xi)$	spatial ordinate of y, shape function
$\psi(\xi)$	spatial ordinate of y_g, shape function
ω	forcing frequency ratio
ω_f	forcing frequency $(\text{rad})(T)^{-1}$
ω_1	small-strain (linear) resonant fundamental frequency of system $(\text{rad})(T)^{-1}$

The stiffness of these springs also varies with depth from the surface. In addition, a strain-dependant nonlinear damping function is employed. Both the stiffness and damping functions match experimental observations qualitatively. After various non-dimensional ordinates are introduced, it is possible to reduce the general system to Duffing's oscillator that has nonlinear damping. It is demonstrated that this Duffing's like system is a generic one that applies for all cases of different pile kinematical boundary conditions.

Three main results are presented in this paper, (i) the small strain (linear) resonant system frequency ω_1, Fig. 2 (or Eq. (61)), (ii) the reduction of this linear frequency with increases in non-dimensional forcing parameter F, Eq. (45) and (iii) the relationship between non-dimensional forcing F and peak ground acceleration (PGA) a_g, Eq. (51). Experimental results obtained elsewhere together with a finite element analysis (FEA) are employed to provide some validation of the small strain formula.

2. Analytical model

Consider the system described in Fig. 1. The pile is surrounded by a "near field" soil stack of layers. A continuum of layers surround the pile. Each layer contains a nonlinear spring, nonlinear dashpot and lumped masses. The effective width

[2] Dimensional units denoted in this paper by bracketed terms, where (F) is force, (L) is length and (T) is time. The dimensionless derived unit (rad) is an angle in radians.

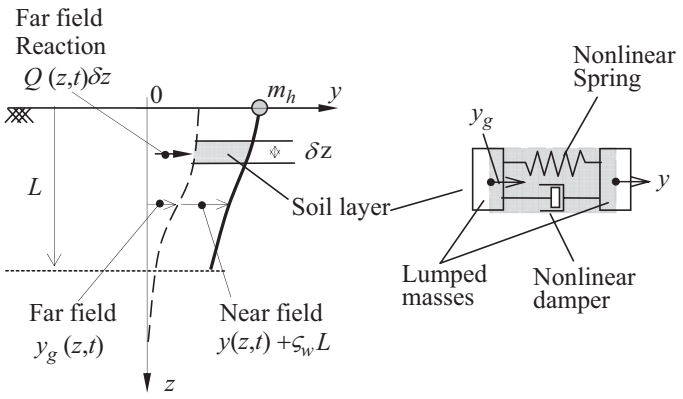

Fig. 1. Analytical model.

of the near-field layer is $\zeta_w L$. The system is sub-structured such that only the near field soil, pile and superstructure mass are considered. For equilibrium to be maintained a set of reactions, $Q(z,t)$, that vary with depth are applied to the near field soil stack. Thus, only the horizontal displacement at the far field–near field interface $y_g(z,t)$ and these reactions $Q(z,t)$ are necessary. The total displacement of the pile is $y_g(z,t)+y(z,t)$ where $y(z,t)$ is a relative horizontal displacement of the pile.

2.1. Using P–y backbone curves

For a range of different soils many different P–y curves proposed by researchers [2–7] and others (too numerous to mention here). The fidelity of these forms of curves to experimental data has been questioned by [7,8]. Results suggest that there is some scatter about these nonlinear trends. This scatter is due to lack of heterogeneity and complex hysteretic nonlinear behaviour of real soils. An example of this scatter is given in [9,10]; where full scale dynamic test data for a pile driven in medium-dense sand is obtained. Dynamic test results show an approximately cubic p–y curve (where p is soil spring load per unit area) complete with a falling part, (cf. Fig. 12 in [9]).

Note that P–y curves for pile-soil springs are normally obtained by applying a load at the head of the pile and recording the displacements of the pile. This is the case for experimental study [9,10]. In this situation the pile ground displacement field y_g is zero and y is the relative displacement of pile and the total displacement of the pile.

More recent work, [11], has suggested that the p–y curves can be loading rate dependant. Thus [11] suggest p–y curves based on static or slow cyclic loading may underestimate the backbone observed under faster cyclic loading. This strain rate hardening in clay soils is clear; in sands this effect seems less marked. The basic shape of these dynamic p–y curves, in [11], is still fairly similar to the *static* p–y curves with a scaling (stretching) of the p axis.

However, for all their limitations P–y curves provide a pragmatic and useful engineering simplification and are used widely in practice. In this paper the form of [7,12] is taken. This is shown in Eq. (1); where P is the soil-spring reaction at depth z, P_u is the ultimate bearing capacity at a depth of z, A is 0.9 a reduction factor for dynamics, k_0 is the initial modulus of subgrade reaction [6], y is the horizontal pile deflection at depth z. This can be re-expressed by assuming that the P_u varies linearly with depth (2); thus it can be expressed in terms of P_{ub} the ultimate bearing capacity at the base of the pile i.e. at depth L. This follows the functional form presented in work of [13–16]. This linear assumption differs from the American Petroleum Institute (API) [12] recommendation that assumes a quadratic variation of P_u with depth for "shallow depths" and a linear variation of P_u with depth for "deep depths". Ref. [16] suggests that the API quadratic variation that was based on a wedge failure mechanism at shallow depths is unduly optimistic compared with other proposed models. Experimental results presented in [17] (cf. Figs. 12 and 14) show a near linearly increase in P_u with depth. Nevertheless, in this paper, a linear variation with depth is assumed mainly because it is computationally simplifying.

$$P(x,z) = s_e A P_u \tanh\left(\frac{k_0 z}{A P_u} y\right) = s_e A P_{ub}\left(\frac{z}{L}\right)\tanh\left(\frac{k_0 L}{A P_{ub}} y\right) \tag{1}$$

$$P_u = P_{ub}\left(\frac{z}{L}\right) \tag{2}$$

For dynamic p–y curves to be incorporated, as [11] suggests, a scale factor s_e to the p axis should be applied. A Taylor series expansion suggests that the tanh function can be expressed as a cubic with higher terms neglected, for a small range of y. However, just expanding and neglecting higher order terms does not often produce the best fit over the problem domain $|y| \le y_p$. The optimal values of linear and nonlinear spring constants k_{w1} and k_{w2} should be sought, in a least square sense, employing Eq. (60) from Appendix B. Thus, the optimal spring coefficients are given by (4) and (5) in terms of k_0, L, y_p and P_{ub}. Note that for $|y| > y_p$ the cubic function falls away from API backbone curve. This can be an advantage as it models degradation of stiffness at large cyclic strains as seen in [9].

In summary, the cubic P–y curve proposed in this paper enforces quartic nonlinear strain energy of the soil.

$$\left(\frac{L}{z}\right)P = s_e A P_{ub} \tanh\left(\frac{k_0 L}{A P_{ub}} y\right) \approx k_{w1} y - k_{w2} y^3 + O(y^5), |y| \le y_p \tag{3}$$

$$k_{w1} = \frac{75}{4y_p^3}\int_0^{y_p}\left(\frac{L}{z}\right)P y \,\mathrm{d}y - \frac{105}{4y_p^5}\int_0^{y_p}\left(\frac{L}{z}\right)P y^3 \,\mathrm{d}y \tag{4}$$

$$k_{w2} = \frac{105}{4y_p^5}\int_0^{y_p}\left(\frac{L}{z}\right)P y \,\mathrm{d}y - \frac{175}{4y_p^7}\int_0^{y_p}\left(\frac{L}{z}\right)P y^3 \,\mathrm{d}y \tag{5}$$

2.2. Potential energy of system

The potential Energy U of this system is composed of two terms: (i) the flexural strain energy of the pile group and (ii) the soil spring stiffness energy. The work done by the far-field soil reactions Q is neglected here as it does not contribute to the subsequent equations of motion. Hysteretic behaviour of springs is not modelled directly as this greatly increases the analytical complexity. However, it is not ignored. The hysteretic behaviour of springs is summed up per cycle and included as an increased nonlinear damping term proposed later. This approach follows work of Voigt and Maxwell described in [18]. This approach is used to determine the variation of soil damping coefficient with strain levels.

$$U = \frac{1}{2}\int_0^L EI(y'' + y_g'')^2 \,\mathrm{d}z + \int_0^L \frac{1}{2}k_{w1}\left(\frac{z}{L}\right)y^2 - \frac{1}{4}k_{w2}\left(\frac{z}{L}\right)y^4 \,\mathrm{d}z \tag{6}$$

If a classical Rayleigh–Ritz spatial–temporal series is adopted, i.e. $y = \sum w_i(t)\phi_i(z)$ then an n degree of freedom nonlinear system is obtained. This is equivalent to a high order (i.e. $2n$) nonlinear ODE. Unfortunately, this is not suitable for an initial investigation into the problem. These high order systems are left for later. In this paper, a first order approximation (a reduced order system) is assumed e.g. using Eq. (7) that result in a nonlinear, single degree of freedom system. This introduces one unknown degree of freedom, w, where wL is the displacement at the top of the pile, and the known degree of freedom, w_g where $w_g L$ is the surface ground horizontal displacement. A non-dimensional variable, ξ, is introduced; it is an ordinate along the pile. Hence primes and double primed variables from now on denote first and second derivative with respect to ξ. The potential energy can be re-expressed as (8): non-dimensional parameters in Eqs. (9) and (10) are introduced.

$$y = Lw(t)\phi(\xi), \quad y_g = Lw_g(t)\psi(\xi), \quad \xi = z/L \tag{7}$$

$$U = \frac{1}{2}\frac{EI}{L}(K_1 w^2 - \frac{1}{2}K_2 w^4 + 2K_g w w_g) + O(w_g) \tag{8}$$

$$\eta_1 = \frac{k_{w1}L^4}{EI}, \quad \eta_2 = \frac{k_{w2}L^6}{EI} \tag{9}$$

$$K_1 = \int_0^1 \phi''^2 + \eta_1 \xi \phi^2 \,\mathrm{d}\xi, \quad K_2 = \eta_2 \int_0^1 \xi\phi^4 \,\mathrm{d}\xi, \quad K_g = \int_0^1 \phi''\psi'' \,\mathrm{d}\xi \tag{10}$$

2.3. Kinetic energy of system

The translational, horizontal, kinetic energy T of the system is defined in (12). The rotational kinetic energy of pile and superstructure mass are neglected in this paper. Parameter m_h is the lumped mass at pile head; i.e. the mass of any structure attached to the top of the pile. m is the mass per unit depth of the pile and soil layer; where m_p is the mass per unit depth of the pile and ρ_s density of the "near field" soil layer. The out of plain breadth of the soil layer is assumed to be $\zeta_b D$. The soil mass for a layer δz is lumped half on the pile and half at the near–far-field boundary. The kinetic energy can be re-expressed, in quadratic form, in terms of degrees of freedom w and w_g by Eq. (13); by using non-dimensional parameters in Eqs. (14) and (15).

$$m = m_p + \tfrac{1}{2}\rho_s \zeta_w \zeta_b LD \tag{11}$$

$$T = \frac{1}{2}\left(m_h(\dot{y}_g(0) + \dot{y}(0))^2 + m\int_0^L (\dot{y}_g + \dot{y})^2 \,\mathrm{d}z\right) \tag{12}$$

$$T = \tfrac{1}{2}mL^3(M\dot{w}^2 + 2M_g\dot{w}\dot{w}_g) + O(\dot{w}_g^2) \tag{13}$$

$$M = \alpha\phi(0)^2 + \int_0^1 \phi^2 \,\mathrm{d}\xi, \quad M_g = \alpha\phi(0)\psi(0) + \int_0^1 \phi\psi \,\mathrm{d}\xi \tag{14}$$

$$\alpha = \frac{m_h}{mL} \tag{15}$$

2.4. Rayleigh dissipative function of system

The damping coefficient of the soil is assumed quadratic in nature, (16); this follows the experimental evidence of [8,19] that suggest the ratio of critical damping is dependent of cyclic soil shear strain amplitude. The strain in the soil spring is $\varepsilon = y/\zeta_w L$. The system Rayleigh dissipative function, R, is given by Eq. (17); frequency s is introduced to aid later simplifications.

$$c = c_1 + c_2\varepsilon^2 \tag{16}$$

$$R = \frac{1}{2}\int_0^L \left(c_1 + c_2\left(\frac{y}{\zeta_w L}\right)^2\right)\dot{y}^2\,\mathrm{d}z = \frac{1}{2}mL^3 s(C_1 + C_2 w^2)\dot{w}^2 \tag{17}$$

$$C_1 = \frac{c_1}{ms}\int_0^1 \phi^2\,\mathrm{d}\xi, \quad C_2 = \frac{c_2}{ms\zeta_w^2}\int_0^1 \phi^4\,\mathrm{d}\xi \tag{18}$$

$$s^2 = \frac{EI}{mL^4} \tag{19}$$

2.5. Equation of motion for system

Thus the Euler–Lagrange–Rayleigh equation of motion (20) can be obtained from (8), (13) and (17). This is re-expressed by the introduction of frequency parameter ω_1 Eq. (21). Also non-dimensional parameters β_1, β_2, β_3, μ_1, μ_2 are introduced, see Eqs. (22) and (23)

$$\ddot{w} + 2(\mu_1 + \mu_2 w^2)\dot{w} + w - \beta_1 w^3 = -\beta_2\ddot{w}_g - \beta_3 w_g \tag{20}$$

$$\omega_1 = s\sqrt{\frac{K_1}{M}} \tag{21}$$

$$\beta_1 = \frac{K_2}{K_1}, \quad \beta_2 = \frac{M_g}{M}, \quad \beta_3 = \frac{K_g}{K_1} \tag{22}$$

$$\mu_1 = \frac{C_1}{2\sqrt{MK_1}}, \quad \mu_2 = \frac{C_2}{2\sqrt{MK_1}} \tag{23}$$

This equation of motion (20) has been further simplified by introducing a time-scale $\tau = \omega_1 t$. Note, subsequently, dots above letters denote differentials with respect to τ i.e. $\dot{w} = dw/d\tau$, $\ddot{w} = d^2w/d\tau^2$ and $\ddot{w}_g = d^2w_g/d\tau^2$.

One final further scaling simplifies this equation. The generalised ordinate w and ground displacement ordinate w_g are re-scaled by (24). This results in Eq. (25), that is a *Duffing's* [20–23] oscillator but with *nonlinear damping*.

$$w = \beta_1^{-1/2}u, \quad w_g = \beta_1^{-1/2}u_g \tag{24}$$

$$\ddot{u} + 2\mu_1(1 + \mu_n u^2)\dot{u} + u - u^3 = -\beta_2\ddot{u}_g - \beta_3 u_g \tag{25}$$

$$\mu_n = \frac{\mu_2}{\mu_1\beta_1} \tag{26}$$

3. Solutions of nonlinear system

3.1. What form should the spatial shape function ϕ take?

This is a difficult question to answer for a number of reasons. Firstly and fairly obviously, it should be stated that the closer ϕ is to the fundamental nonlinear mode shape, the more accurate this single degree of freedom model will be. Secondly, the relative stiffness of soil to pile governs this mode shape ϕ. There is also the problem that if the reduction in stiffness due to nonlinearity significantly influences this pile/soil spring stiffness ratio it will influence ϕ. Hence the accuracy of the simplified model is likely to reduce as response amplitude increases. Finally, the boundary conditions to which the pile is subject govern the form of ϕ significantly. The boundary conditions at the bottom (toe) of the pile are governed by the soil layer at this level. The boundary conditions at the top (head) are governed by the pile cap, etc.

So how about employing the systems first linear natural mode for ϕ? This would represent a projection of the nonlinear system onto a truncated linear modal basis. It would give a very good approximation at low amplitudes. It would be useful to observe how the soil/pile linear stiffness ratio, η_1, influences the linear fundamental natural mode ϕ.

First let us compute an n degree of freedom estimate of the linear natural modes. A series of shifted Legendre polynomials, P_n are used. These are defined to be orthogonal over range zero to one. The pile displacement y can be defined

(28) in term of vector of shape functions $\boldsymbol{\theta}_1$ and $\boldsymbol{\theta}_2$ can be defined as (27). Essentially, the q generalised coordinates $\mathbf{w}_q \in \mathbb{R}^q$ will be constrained by the boundary conditions leaving n unconstrained generalised coordinates $\mathbf{w} \in \mathbb{R}^n$.

$$\boldsymbol{\theta}_1^{\mathrm{T}} = [P_{n+q-1}, P_{n+q-2}, \ldots, P_n] \in \mathbb{R}^q, \boldsymbol{\theta}_2^{\mathrm{T}} = [P_{n-1}, P_{n-3}, \ldots P_0] \in \mathbb{R}^n \tag{27}$$

$$y = L(\boldsymbol{\theta}_1^{\mathrm{T}}\mathbf{w}_q + \boldsymbol{\theta}_2^{\mathrm{T}}\mathbf{w}) \tag{28}$$

For a pile without pile cap the boundary conditions are $y''(1) = y'''(1) = 0$; these are represented in Eq. (29). For the case of a pile with pile cap a further boundary condition is included $y'(0) = 0$; these are represented in Eq. (30). Thus, the shape function vector $\boldsymbol{\phi}$ that satisfies these boundary conditions is given by (31). The only requirement for use of this result is that the boundary condition block matrix $\mathbf{A}_1 \in \mathbb{R}^{q\times q}$ should not be singular. In the case of singular $\mathbf{A}_1$ reordering the Legendre polynomials will normally help to obtain a non-singular $\mathbf{A}_1$. Note that re-ordering the rows or columns of general matrix $\mathbf{A}$ cannot change its rank but it can change the rank of a sub-matrix of $\mathbf{A}$; and this is what is proposed here. Block matrix $\mathbf{A}_2 \in \mathbb{R}^{q\times n}$ is generally not square. For clarity, Appendix A gives a worked example of Eqs. (29) and (31).

$$\begin{bmatrix} \theta''(1)_1^{\mathrm{T}} & \theta''(1)_2^{\mathrm{T}} \\ \theta'''(1)_1^{\mathrm{T}} & \theta'''(1)_2^{\mathrm{T}} \end{bmatrix} \begin{bmatrix} \mathbf{w}_q \\ \mathbf{w} \end{bmatrix} = [\mathbf{A}_1 \;\; \mathbf{A}_2] \begin{bmatrix} \mathbf{w}_q \\ \mathbf{w} \end{bmatrix} = \mathbf{0} \tag{29}$$

$$\begin{bmatrix} \theta'(0)_1^{\mathrm{T}} & \theta'(0)_2^{\mathrm{T}} \\ \theta''(1)_1^{\mathrm{T}} & \theta''(1)_2^{\mathrm{T}} \\ \theta'''(1)_1^{\mathrm{T}} & \theta'''(1)_2^{\mathrm{T}} \end{bmatrix} \begin{bmatrix} \mathbf{w}_q \\ \mathbf{w} \end{bmatrix} = [\mathbf{A}_1 \;\; \mathbf{A}_2] \begin{bmatrix} \mathbf{w}_q \\ \mathbf{w} \end{bmatrix} = \mathbf{0} \tag{30}$$

$$y = L\mathbf{w}^{\mathrm{T}}\boldsymbol{\phi}, \quad \boldsymbol{\phi} = (\boldsymbol{\theta}_2^{\mathrm{T}} - \boldsymbol{\theta}_1^{\mathrm{T}}\mathbf{A}_1^{-1}\mathbf{A}_2)^{\mathrm{T}} \tag{31}$$

Note that this approach is more subtle than conventional finite element analysis (FEA). Here, the shape functions are continuous across the entire problem domain. This is more similar to boundary element method. Degrees of freedom (dofs) are amplitudes of shape functions here. This contrasts with FEA, where degrees of freedom are general displacements or rotations at nodal positions. Thus, in FEA, dofs at boundaries must be constrained to satisfy boundary conditions. Here however, dofs are shape function amplitudes, thus it is necessary and sufficient to constrain almost *any* q dofs; (with the proviso that these constrained dofs do not result in singular $\mathbf{A}_1$).

Given this series expansion for the pile displacement the Lagrangian Π can be defined thus;

$$\frac{\Pi}{mL^3} = \frac{1}{2}\left(\alpha(\dot{\mathbf{w}}^{\mathrm{T}}\boldsymbol{\phi}(0))^2 + \int_0^1 (\dot{\mathbf{w}}^{\mathrm{T}}\boldsymbol{\phi})^2\,\mathrm{d}\xi\right) - \frac{1}{2}s^2\int_0^1 (\mathbf{w}^{\mathrm{T}}\boldsymbol{\phi}'')^2 + \eta_1\xi(\mathbf{w}^{\mathrm{T}}\boldsymbol{\phi})^2\,\mathrm{d}\xi \tag{32}$$

By employing the Euler–Lagrange equations to Π the dynamic matrix $\mathbf{D}$ can be obtained; Eq. (34). The eigenvectors of $\mathbf{D}$ are the natural linear modes of vibration of the pile–soil system.

$$\mathbf{K} = \int_0^1 \boldsymbol{\phi}''\boldsymbol{\phi}''^{\mathrm{T}} + \eta_1\xi\boldsymbol{\phi}\boldsymbol{\phi}^{\mathrm{T}}\,\mathrm{d}\xi, \quad \mathbf{M} = \alpha\boldsymbol{\phi}(0)\boldsymbol{\phi}(0)^{\mathrm{T}} + \int_0^1 \boldsymbol{\phi}\boldsymbol{\phi}^{\mathrm{T}}\,\mathrm{d}\xi \tag{33}$$

$$\mathbf{D} = s^2\mathbf{M}^{-1}\mathbf{K} \tag{34}$$

The first linear natural frequency ω_1 vs. parameters η_1 and α is displayed in Fig. 2. The first mode profile can be employed to determine moments and shear force functions. These functions are display graphically in Figs. 3 and 4. These moment diagrams are very similar, qualitatively, to those obtained experimentally [8–10,19] and are consistent with other theoretical work [24]. These conditions apply to case of homogeneous soil profile with depth. The presence of stiff soil layers at the pile base that are overlain with softer, more flexible, soil layers would suggest a different set of support boundary conditions not considered here. Though, in principle, the approach would be the same with some small modifications for these different kinematic constraints.

A good analytical approximation to Fig. 2 is given in Appendices B–D, see Eq. (61). In addition a good approximation to the linear first mode shape is presented. These formulae provide an alternative to employing Fig. 2 but are not used in subsequent analysis in this paper.

From these figures the influence of η_1 on the deflected shape is significant. However, for a given η_1, the reduction in soil-springs stiffness that is due to nonlinear behaviour of the soil changes the deflected shape a little. This is because only a change in the order of magnitude of η_1 effects the first mode shapes significantly. Thus, there is evidence to suggest, in this case, that the proposed single shape function (7) is a reasonable first approximation to the nonlinear natural mode. In addition, this is evidence that suggests the use of a single degree of freedom reduced order model is valid. The exact form of this shape function is obtained numerically by either eigenvalue analysis of matrix (34) or by using the very good approximation given in Appendices C–E.

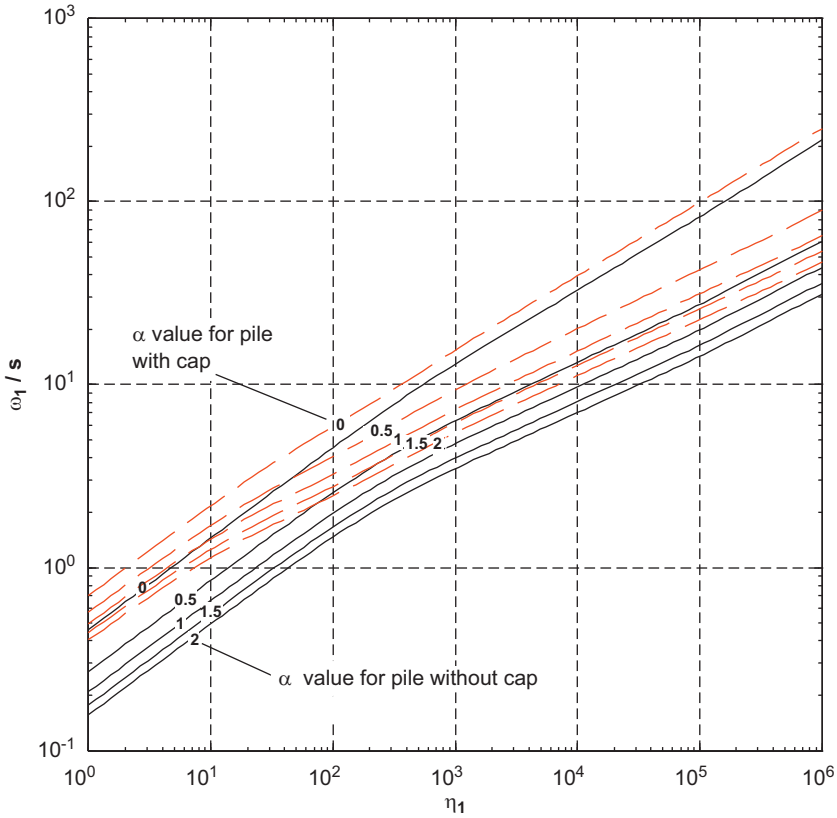

Fig. 2. Linear fundamental frequency ω_1 vs. soil to pile stiffness ratio η_1.

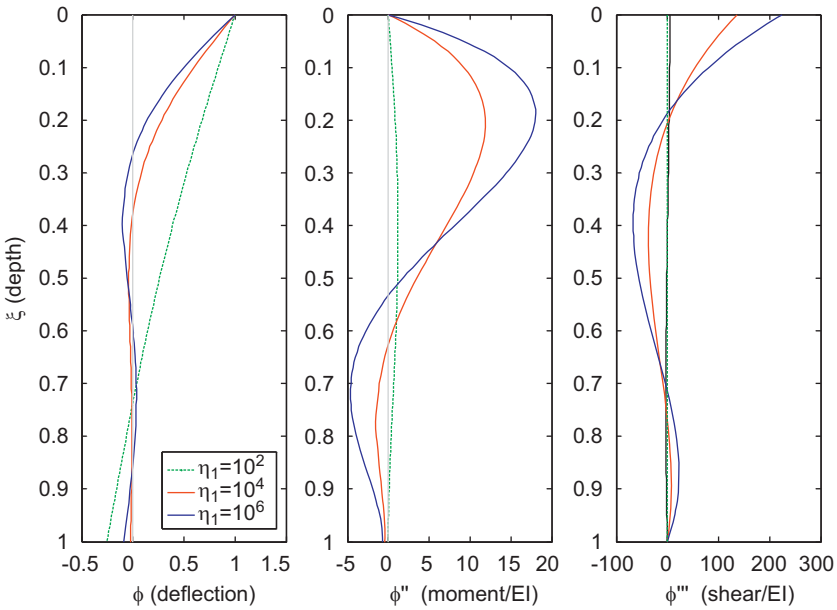

Fig. 3. First mode for pile without cap.

3.2. Nonlinear resonance curve

In order to obtain a nonlinear resonance curve the system is driven by harmonic forcing, hence the equation of motion is (35). F is the amplitude of the forcing in non-dimensional equation. The non-dimensional forcing frequency ratio ω

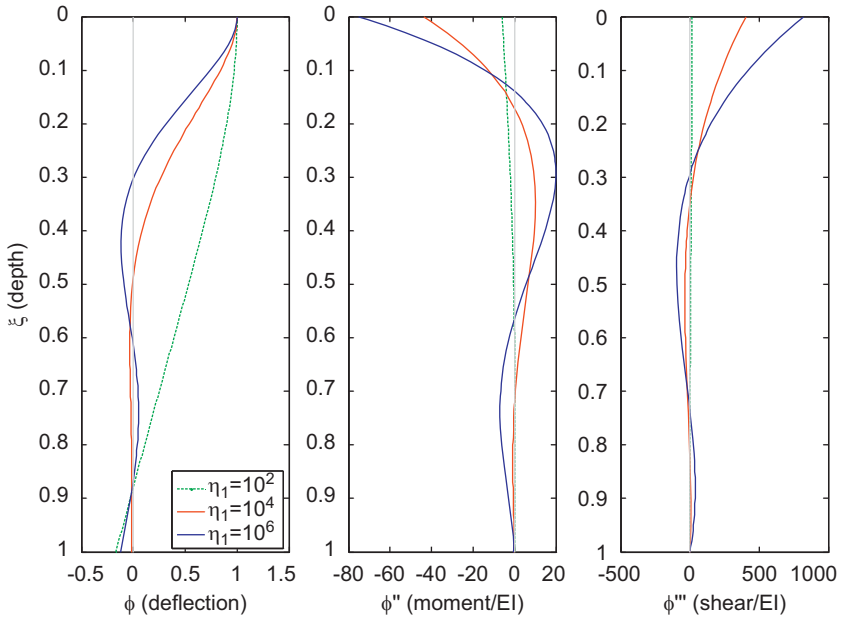

Fig. 4. First mode for pile with cap.

equals the ratio ω_f/ω_1 where ω_f would be the dimensional forcing frequency.

$$\ddot{u} + 2\mu_1(1+\mu_n u^2)\dot{u} + u - u^3 = F\sin(\omega\tau), \quad \omega = \frac{\omega_f}{\omega_1} \tag{35}$$

The parameters β_1, β_2 and β_3 are dependant on the shape functions ϕ and ψ that are themselves influenced by the boundary conditions (constraints) of the pile. However it appears, at first glance, that these play no part in Eq. (35).

In this paper, the nonlinear resonant frequency of the system is defined as the frequency at which extremum (maximum) in the nonlinear resonance curve occurs. The location of this extremum is a difficult problem. It requires the solution of the nonlinear ordinary differential Eq. (35). Unfortunately, there are no analytical approaches that are able to obtain this solution, in general. Thus, one is left with the choice of semi-analytical-approximate methods such as harmonic balance, multi-scales, averaging methods [25,26] or fully numerical continuation approaches [27,28]. In this paper, a hybrid of a higher order harmonic balance and numerical continuation is used.

A second order estimate of the solution to this nonlinear equation can be obtained by assuming that the solution takes the form (36) [29–31]. Higher order estimate were considered but found unnecessary for the sole objective of determining the maxima of the resonance curves. This trial solution (36) is substituted into system (35). The coefficients of $\sin\omega\tau$, $\cos\omega\tau$, $\sin 3\omega\tau$ and $\cos 3\omega\tau$ are evaluated and balanced on each side of the equation; and this results in four simultaneous nonlinear algebraic equations (37)–(40). The classical harmonic balance approach [32] is employed. This neglects higher order terms.

$$u = a_1\cos\omega\tau + a_2\sin\omega\tau + a_3\cos 3\omega\tau + a_4\sin 3\omega\tau \tag{36}$$

$$\begin{aligned}&(\tfrac{1}{2}a_2^3 - \tfrac{1}{2}a_2^2a_4 + (\tfrac{1}{2}a_1^2 - a_1a_3 + a_3^2 + a_4^2)a_2 + \tfrac{1}{2}a_1^2a_4)\omega\mu_n\mu_1 + 2\mu_1\omega a_2 - a_1\omega^2 \ldots\\ &\quad +\tfrac{3}{4}a_2^2(a_3 - a_1) - \tfrac{3}{2}a_1a_2a_4 - \tfrac{3}{4}a_1^3 - \tfrac{3}{4}a_1^2a_3 + (1 - \tfrac{3}{2}a_4^2 - \tfrac{3}{2}a_3^2)a_1 = 0\end{aligned} \tag{37}$$

$$\begin{aligned}&(\tfrac{1}{2}a_2^2(a_3 - a_1) - a_1a_2a_4 - \tfrac{1}{2}a_1^3 - \tfrac{1}{2}a_1^2a_3 - a_1a_4^2 - a_1a_3^2)\omega\mu_1\mu_n - 2\mu_1\omega a_1 \ldots\\ &\quad -\omega^2a_2 - \tfrac{3}{4}a_2^3 + \tfrac{3}{4}a_2^2a_4 + (1 - \tfrac{3}{2}a_3^2 - \tfrac{3}{4}a_1^2 + \tfrac{3}{2}a_1a_3 - \tfrac{3}{2}a_4^2)a_2 - \tfrac{3}{4}a_1^2a_4 - F = 0\end{aligned} \tag{38}$$

$$\begin{aligned}&(\tfrac{3}{2}a_3^2a_4 + \tfrac{3}{2}a_4^3 - \tfrac{1}{2}a_2^3 + \tfrac{3}{2}a_1^2a_2 + 3a_1^2a_4 + 3a_2^2a_4)\omega\mu_1\mu_n + 6\omega\mu_1a_4 \ldots\\ &\quad -9a_3\omega^2 + a_2^2(\tfrac{3}{4}a_1 - \tfrac{3}{2}a_3) - \tfrac{3}{4}a_3a_4^2 - \tfrac{3}{2}a_1^2a_3 - \tfrac{1}{4}a_1^3 - \tfrac{3}{4}a_3^3 + a_3 = 0\end{aligned} \tag{39}$$

$$\begin{aligned}&((\tfrac{3}{2}a_1 - 3a_3)a_2^2 - \tfrac{3}{2}a_3^3 - 3a_1^2a_3 - \tfrac{3}{2}a_3a_4^2 - \tfrac{1}{2}a_1^3)\omega\mu_1\mu_n - \tfrac{3}{4}a_1^2a_2 \ldots\\ &\quad -\tfrac{3}{2}a_2^2a_4 - \tfrac{3}{2}a_1^2a_4 + a_4 - \tfrac{3}{4}a_3^2a_4 - 9\omega^2a_4 - 6\omega\mu_1a_3 + \tfrac{1}{4}a_2^3 - \tfrac{3}{4}a_4^3 = 0\end{aligned} \tag{40}$$

The solution of Eqs. (37)–(40) required a numerical procedure, such as Gauss–Newton ([33], function *fsolve*). However, while a single solution to these equations is straightforward (with the correct numerical toolbox) the process of obtaining a nonlinear resonance curve does require the addition of an arc-length continuation condition. Eq. (41) is a linear predictor based on initial point on a path $\mathbf{q}_i=[a_1,a_2,a_3,a_4,\omega]^{\mathrm{T}}$, step size Δ and an normalised path vector $\delta\mathbf{q}_i=[\delta a_1,\delta a_2,\delta a_3,\delta a_4,\delta\omega]^{\mathrm{T}}$. Vector $\tilde{\mathbf{q}}_{i+1}$ represents the first estimate of the next point along the continued path. Eq. (42) is solved together with Eqs. (37)–(40); it ensures that solution must be normal to the path vector $\delta\mathbf{q}_i$. Essentially these equations act as a correction to the prediction (41). Once a solution is obtained this becomes the new $\mathbf{q}_{i+1}$. An update of the vector is made $\delta\mathbf{q}_{i+1}$ based on linear extrapolation of the previous points $\mathbf{q}_{i+1}$ and $\mathbf{q}_i$ (43).

$$\tilde{\mathbf{q}}_{i+1}=\mathbf{q}_i+\Delta\delta\mathbf{q}_i \tag{41}$$

$$(\mathbf{q}_i-\tilde{\mathbf{q}}_{i+1})^{\mathrm{T}}\delta\mathbf{q}_i=0 \tag{42}$$

$$\delta\mathbf{q}_{i+1}=\frac{(\mathbf{q}_{i+1}-\mathbf{q}_i)}{\|\mathbf{q}_{i+1}-\mathbf{q}_i\|_2} \tag{43}$$

3.2.1. Values for strain dependant ratio of critical damping

In order to solve these harmonic balance equation damping parameters μ_1 and μ_n must be specified. A significant amount of experimental work [34–37] and others has been performed on soils in order to determine the relationship between damping ratio and cyclic shear strain amplitude. Most soils have a damping ratio of 0.01–0.02 at low strain levels (of the order of 10^{-5}) this grows approximately quadratically to about 0.15–0.25 at larger strain levels (of the order of 10^{-2}).

In theory it is possible to work from Eq. (18) and (23) to determine μ_1 and μ_n. However, a set of parameters need to be assigned and these require, critically, knowledge of the width of the near-field zone ζ_w and this is not well defined at present. In addition mode shape ϕ is required. This suggests that pile boundary conditions would influence the damping parameters in (35). However, it would be beneficial to keep (35) independent of ϕ as far as possible.

So an alternative approach is sought. Note that the normalised cubic stiffness term of (35) is bounded physically by $|u|\leq 1$. Exceeding this limit is considered failure of the soil. Further investigations into velocity bounds of the catchment basins can be made by applying techniques in [38,39]. Thus, it is assumed that the maximum damping of the soil is achieved at this maximum displacement. It is assumed that at this level of normalised deformation that the system damping reaches $\mu_{\max}$. Thus, the nonlinear damping parameter μ_n is defined by (44).

$$\mu_n=\frac{\mu_{\max}}{\mu_1}-1 \tag{44}$$

Fig. 5 displays an example of the nonlinear resonance curves for a range of forcing amplitudes. The vertical axis, in this figure, represents the magnitude (the supremum norm, $\|u\|_\infty$) of the solutions.

This system shows a classical softening response with the resonance peak that falls over to the left with increasing amplitude of forcing. At larger forcing amplitudes the response curves become multivalued; having a high amplitude solution, a low amplitude solution and an unstable (saddle) solution. A pair of fold bifurcations (turning points) bound this unstable solution. The presence of low and high amplitude coexisting solutions can result in sudden jumps to resonance [40], from low to high amplitude with small changes in forcing frequency.

The extrema are denoted by circles in this figure, these extrema are nonlinear resonant frequencies of the system, ω_r.

3.3. Nonlinear resonant frequency relationship

Fig. 6(a) is obtained when the resonant frequencies ω_r are plotted against forcing amplitude F for various μ_n. An optimal multidimensional polynomial (45) is fitted to these graphs in (F,μ_n), see Appendix B. Note that μ_1 shall be, in this paper, universally assumed 0.01. This optimal least square approximation is very good for engineering purposes.

$$\frac{\omega_r}{\omega_1}\simeq\left(1-7.163F+0.1433\mu_nF-0.6578\mu_nF^2-4.808\times10^6\left(\frac{F}{\mu_n}\right)^3\right)\geq 0.6 \tag{45}$$

Hence with a knowledge of the linear natural frequency of the system ω_1, that is a function of pile and soil parameters, it is possible to obtain an estimate of the nonlinear resonant frequency ω_r by using formula (45). Note that this equation suggests a bound on nonlinear resonant frequency $\omega_1\geq\omega_r\geq 0.6\omega_1$.

It is also worthwhile obtaining a multidimensional least squares polynomial fit for the maximum amplitude of the response solution $\|u\|_\infty$ in (F,μ_n). This is obtained in a similar fashion and is given by Eq. (46) and is displayed in Fig. 6(b). Again, this is a very good fit for engineering purposes.

$$\|u\|_\infty\simeq 24.84F-531.9F^2+4564F^3+2.363\times10^4\left(\frac{F}{\mu_n}\right)^2+5.133\left(\frac{F}{\mu_n}\right)^{1/2}\leq 1 \tag{46}$$

The ratio of peak response to forcing amplitude $\|u\|_\infty/F$, known as the nonlinear amplification factor, is displayed in Fig. 7.

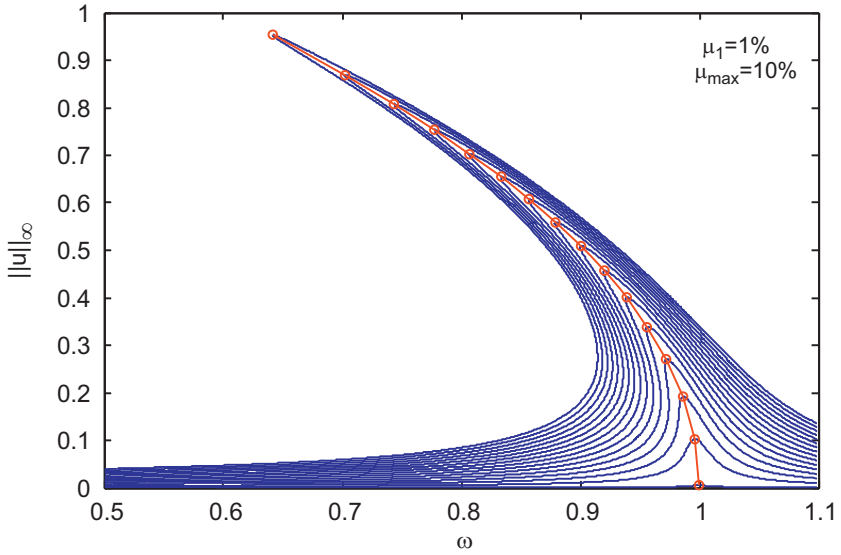

Fig. 5. Example of nonlinear resonance curves.

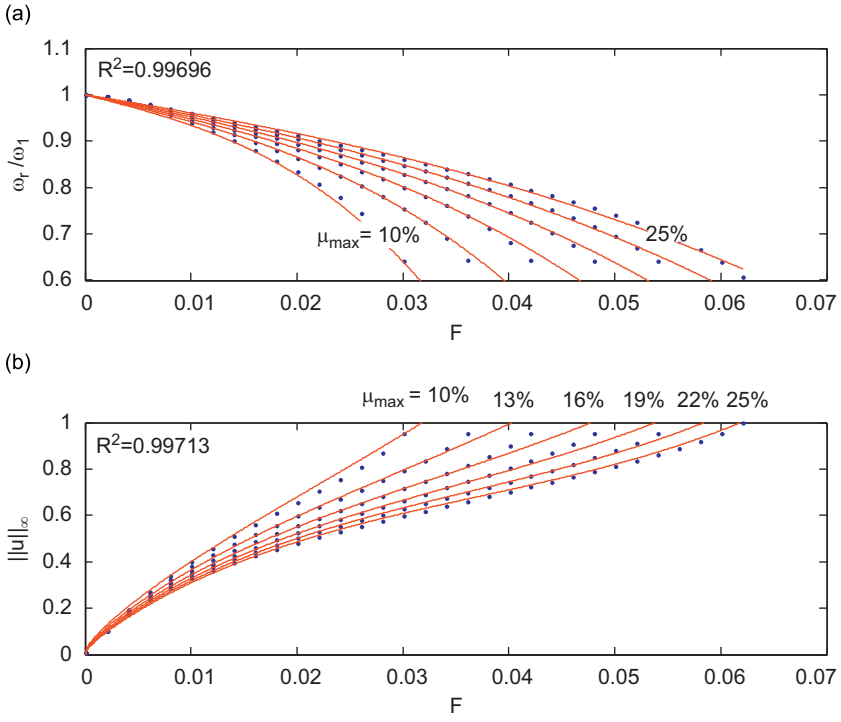

Fig. 6. (a) Variation of nonlinear resonant frequency with forcing amplitude F and (b) variation in the maximum response of solution with F. In both cases ($\mu_1 = 1\%$).

3.4. *Relating non-dimensional forcing amplitude F to far-field PGA*

The key result, hitherto, is Eq. (45). From this the nonlinear resonant frequency can be determined in terms of the linear (very small soil-strain) fundamental natural frequency ω_1. This linear frequency ω_1 can be read from Fig. 2 (or Eq. (61)) for various mass ratios α and linear soil/pile stiffness ratios η_1. Hence, with (45) and Fig. 2 (or Eq. (61)) it is possible to determine the nonlinear resonant frequency of the pile-soil system in terms of parameters (i) mass ratio α, (ii) linear soil to pile stiffness η_1, (iii) frequency s, (iv) large strain damping μ_n and (v) non-dimensional forcing amplitude F.

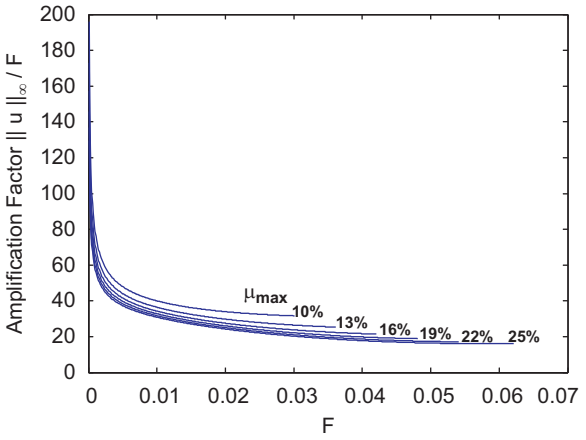

Fig. 7. Nonlinear amplification factor for system.

Note, however, F is not a natural parameter; so it would be beneficial, for the practicing engineer, to express this in terms of some dimensional quantity. By considering Eqs. (35) and (25) it is clear that the forcing function adopted in the study thus far is equivalent to a ground motion u_g that can be obtained by equating these equations. Scaled ground motion w_g and far-field ground motion $\ddot{y}_g(\xi,t)$ can subsequently be determined by using (7) in terms of F, thus

$$\ddot{y}_g(\xi,t) = \omega_1^2 L \frac{\omega^2 F}{\beta_1^{1/2}(\beta_2\omega^2 - \beta_3)} \sin(\omega_f t)\psi(\xi) \tag{47}$$

Hence, given a surface far-field peak ground acceleration (PGA) of $a_g = \max(\ddot{y}_g(1,t))$, the correspondent value of non-dimensional forcing amplitude F, at resonance, is given by (48).

$$F = \left(\frac{a_g}{\omega_1^2 L}\right)A, \quad A = \beta_1^{1/2}\left(\beta_2 - \beta_3\left(\frac{\omega_1}{\omega_r}\right)^2\right) \tag{48}$$

So, clearly, one final equation is also required; an expression for A in terms of system parameters η_1, η_2 and α.

The system non-dimensional parameters β_2 and β_3 can be evaluated in terms of parameters α and η_1 by using Eqs. (22), (9), (10), (14) and (15). An estimate of the far-field ground displacement function ψ is required. In this paper a linear function is assumed, Eq. (49).

$$\psi = 1 - \xi \tag{49}$$

Richart et al. [41] derived theoretical estimates for the variation in amplitude with depth for both seismic Rayleigh and Love waves. While these relationships are generally nonlinear, they are linear in the very shallow superficial layers of soil in which the pile is embedded. Hence, linear (49) is reasonable.

Therefore, in this case, Eq. (48) can expressed as the following Eq. (50).

$$A = \eta_2^{1/2} f(\eta_1,\alpha), \quad f(\eta_1,\alpha) = \left(\frac{\int_0^1 \xi\phi^4\,\mathrm{d}\xi}{\int_0^1 \phi''^2 + \eta_1\xi\phi^2\,\mathrm{d}\xi}\right)^{1/2}\left(\frac{\alpha + \int_0^1 \phi\psi\,\mathrm{d}\xi}{\alpha + \int_0^1 \phi^2\,\mathrm{d}\xi}\right) \tag{50}$$

α has a second order influence; and this is born out by numerical investigations. By employing a least square fit that is reasonably good, $R^2 = 0.98$, the following expression is obtained (51). The coefficient b_0 for this regression is (i) $b_0 = 1.851$ (pile with cap) and (ii) $b_0 = 1.731$ (for pile without cap).

$$F = b_0\left(\frac{a_g}{\omega_1^2 L}\right)\sqrt{\frac{\eta_2}{\eta_1}} \tag{51}$$

4. Comparison with experimental centrifuge results [9,10]

4.1. Comparison with linear experimental results

It is important to ensure that the formulae presented are of the right order. Researchers [42–45] present interesting experimental work on various failure mechanisms of piled structures. Experimental evidence is also available in the literature for determining the linear resonance frequency. Work presented in [9,10] describes both full scale and centrifuge studies on the cyclic dynamic lateral pile behaviour in a cohesionless soil. These tests result provide information necessary as an initial validation of the linear resonant frequency ω_1. From the test data, API curves can be estimated using the

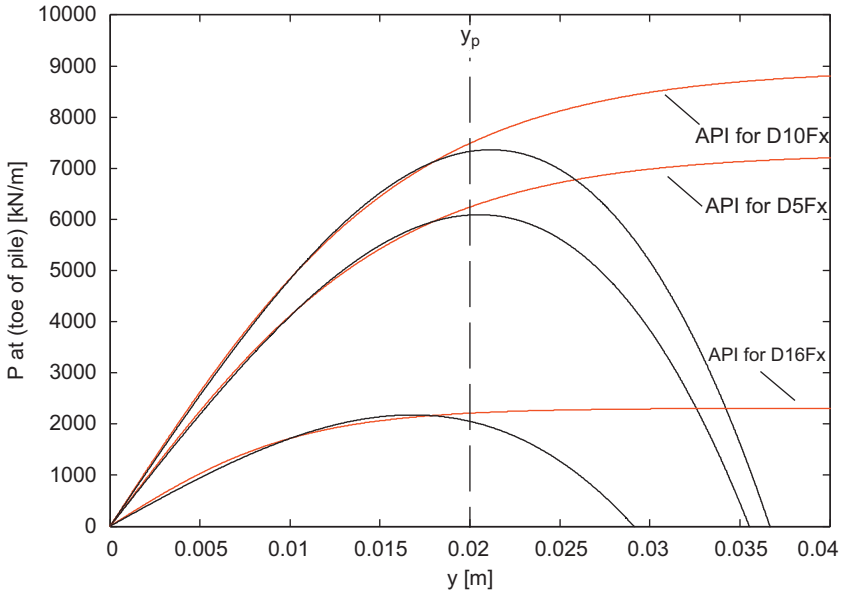

Fig. 8. Comparison of API curves for experimental data and cubic least square estimate of API using Eqs. (3)–(5).

Table 1
Comparison of experimental, theoretical and FEA estimates of natural frequency.

Ting et al. [9,10]	Back analysis from experimental data+Eq. (60)							FEA
Test series	$\omega_1/2\pi$ (Hz)	k_{w1} (kN m^{-2})	k_{w2} (kN m^{-4})	η_1 (−)	η_2 (−)	α (−)	$\omega_1/2\pi$ (Hz)	$\omega_1/2\pi$ (Hz)
D5Fx	1.63	4.27E5	3.19E8	3.64E4	3.34E9	0.018	1.8	1.77
D10Fx	2.13	4.99E5	3.49E8	6.57E4	7.64E9	0.021	2.0	1.84
D16Fx	1.56	1.99E5	2.41E8	3.18E5	7.37E9	0.017	1.5	1.61

relative density of the sand. Fig. 8 show these P–y curves for the toe of the pile, for three data sets presented in [9]. Eqs. (4) and (5) are employed to determine the spring constants k_{w1} and k_{w2}. These allow a back calculation of soil/pile stiffness parameters η_1 and η_2. These are displayed in Table 1. A graphical comparison of the frequency estimates is displayed in Fig. 9. Parameters ζ_w and ζ_b are required to evaluate the soil mass contribution to the dynamics of the pile. Model updating was employed to determine a best value of $\zeta_w\zeta_b$ which as about 22. If $\zeta_b = 2$, that out-of-plane breath is two diameters, then the in-plane width of the near field is 11 diameters; or 5.5 diameters on both sides of the pile. The interaction effects between multiple piles, is thought to be negligible at about 6 diameters [46,47]. While this seems of the right order, these observations are only for the static loading and slow cyclic loading. Group pile interaction under dynamic lateral loading may well extend beyond 6 diameters. Further, experimental work is required here.

The FE analysis involves the pile modelled as Euler-beam elements, the soil springs spaced at 1 m depths spacing. Spring stiffnesses vary with depth linearly. The lumped soil masses at 1 m depth spacing (based on $\zeta_w\zeta_b = 22$) and added along with the lumped mass the top of the pile. The modal analysis is linear. The difference between the FEA results and theoretical estimates are due to slight differences in modelling. For example FEA uses discrete springs while the theoretical estimate, Fig. 2 (or Eq. (61)) uses a continuum of springs. It can be inferred are that Fig. 2 (or Eq. (61)) is quite good as a frequency estimate for this data set.

4.2. *Application of nonlinear formula to this example*

Using the data from the previous section it is possible to employ Eqs. (51) and (45) to obtain an estimate of the variation of nonlinear resonant frequency vs. PGA. Fig. 10 displays these estimates. Validation of these results requires detailed experimental work not available in [9,10].

5. Discussion and conclusions

The paper presents good formulae for both linear and nonlinear resonant frequency of a pile-soil system. It has been demonstrated, quantitatively, how this resonant frequency reduces with increasing amplitude of seismic ground motion. The paper characterises the performance of this system in general and highlights the possibility of multiple (low and high)

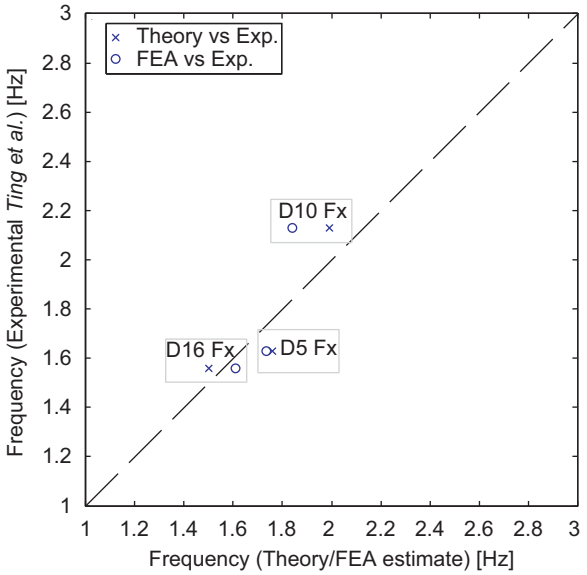

Fig. 9. Comparison of experimental linear resonant frequency with theoretical resonant frequency using Eq. (61) and FEA results.

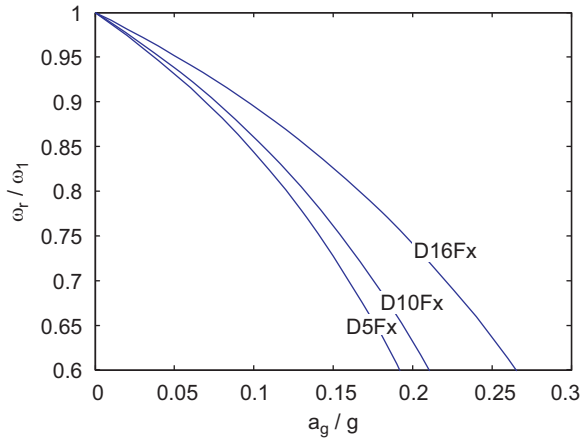

Fig. 10. Example of nonlinear resonant frequencies for Ting's [9,10] examples ($\mu_1 = 0.01, \mu_n = 24$).

amplitude solutions at certain frequencies. This nonlinear phenomenon is very easily overlooked in conventional nonlinear finite element analysis. Note that multiple solutions at a particular frequency is not possible in a linear systems; thus the presented modelling highlights some of the complexity introduced by nonlinearity of the soil. The formulae can be easily incorporated into design as part of 'code based' equations and charts or as part of the background validation of a nonlinear finite element analysis. Both are useful and timely at present.

An estimate of nonlinear resonant frequency of the floating pile system is presented; using Eqs. (45) and Fig. 2 (or Eq. (61)). The linear components of these, Fig. 2 (or Eq. (61)), is compared with experimental evidence and is found to be of the right order. Experimental work [48,49] show that the resonant frequency does drop with increasing forcing amplitude as the theoretical model suggest. Further experimental work would be very helpful. Experimental care is required to determine both upper and lower branches of the resonance curves at higher amplitudes.

Eq. (51) allows the relationship between PGA and nonlinear resonant frequency to be estimated. An example application of this is shown in Fig. 10. Experimental validation of this is required. Note that these estimates are a worst case scenario, i.e. a harmonic ground motion, with a frequency that excites the pile structure resonantly. Further calibration may be required to generalise this result to the case of more typical accelerogram ground motion.

Future work on a higher order nonlinear model would be helpful to validate the accuracy of the proposed reduced order model of the pile. Although initial evidence presented, from variation in mode shape with soil stiffness, suggests that only an order of magnitude change in soil stiffness influences the nonlinear mode shape. Thus, this low order model may be quite good.

The introduction of varying width of near-field soil layer would allow the model to have a variation in effective soil mass with depth. It is likely that more soil motion occurs near the pile head and thus more mass should be included here. It is highly desirable to perform careful experimental studies to ascertain the volume of soil that should be included in the near-field.

Acknowledgement

The author acknowledges the support of the University of Bristol. *Deo Gratias.*

Appendix A. Example of obtaining set of orthogonal polynomials that satisfy the boundary conditions

The following is an illustrative example of low order for the sake of clarity. The actual formulation used in computations is this paper is much higher order. Consider Eqs. (27) and (28); for this example let us employ two constraints $y''(1) = y'''(1) = 0$ i.e. zero shear and moment at the foot of the pile. We shall use two constrained generalised coordinates q=2 (matching the two boundary conditions) and three unconstrained generalised coordinates n=3. Hence

$$\boldsymbol{\theta}_1 = \begin{bmatrix} 1 + 70\xi^4 - 140\xi^3 + 90\xi^2 - 20\xi \\ 20\xi^3 - 30\xi^2 + 12\xi - 1 \end{bmatrix}, \quad \boldsymbol{\theta}_2 = \begin{bmatrix} 1 + 6\xi^2 - 6\xi \\ 2\xi - 1 \\ 1 \end{bmatrix} \tag{52}$$

Substituting the boundary conditions into these expression results in Eq. (29), which here is explicitly (53); then the block matrices $\mathbf{A}_1$ and $\mathbf{A}_2$ are obtain directly.

$$\begin{bmatrix} 180 & 60 & 12 & 0 & 0 \\ 840 & 120 & 0 & 0 & 0 \end{bmatrix} \begin{bmatrix} w_{q1} \\ w_{q2} \\ w_1 \\ w_2 \\ w_3 \end{bmatrix} = \begin{bmatrix} 0 \\ 0 \end{bmatrix} \tag{53}$$

In this example $\mathbf{A}_1 \in \mathbb{R}^{2\times 2}$ is invertible. However, taking a look at the block of four zero in block matrix $\mathbf{A}_2$ it is clear that in another example of boundary conditions $\mathbf{A}_1$ might not have been invertible. The trick here was to place the Legendre polynomials in reverse order. So generally, this method may require some reordering (or some permutation) of the orthogonal function such that $\mathbf{A}_1$ (that must be square) is invertible. The resulting set of 3 orthogonal functions are obtained by Eq. (31). These three functions satisfy the boundary conditions.

$$\boldsymbol{\phi} = \begin{bmatrix} \frac{7}{5} + 21\xi^2 - \frac{56}{5}\xi + \frac{7}{2}\xi^4 - 14\xi^3 \\ 2\xi - 1 \\ 1 \end{bmatrix} \tag{54}$$

Note, finally, that the rank of $\mathbf{A}_1$ must be equal to the number of constraints q.

Appendix B. Multi-dimensional least square estimate

Let the least square estimate of $w(x_1, \ldots, x_n)$ be $\tilde{w}$ and let it take the form given in Eq. (55); where coefficients and polynomial function is defined by $\mathbf{b}$ and $\mathbf{X}$, respectively, Eq. (56). The square error E between this least square estimate and the exact expression is stated in Eq. (57).

$$\tilde{w} = \mathbf{b}^{\mathrm{T}}\mathbf{x} \tag{55}$$

$$\mathbf{b}^{\mathrm{T}} = [b_0, b_1, b_2, b_3, b_4, b_5, b_6, b_7, \ldots],$$

$$\mathbf{x}^{\mathrm{T}} = [1, x_1, \ldots, x_n, \ldots, x_1^m, \ldots, x_n^m, x_1x_2, \ldots] \tag{56}$$

$$E = \int \cdots \int (\tilde{w} - w)^2 \, \mathrm{d}x_1 \cdots \mathrm{d}x_n = \int \cdots \int (\mathbf{b}^{\mathrm{T}}\mathbf{x} - w)^2 \, \mathrm{d}x_1 \cdots \mathrm{d}x_n \tag{57}$$

The least square error, with respect to the coefficients $\mathbf{b}$ of the multidimensional polynomial is obtained by differentiation with respect to $\mathbf{b}$, Eq. (58). Thus, the optimal coefficients are given by (60).

$$\frac{\partial E}{\partial \mathbf{b}} = 2\mathbf{H}\mathbf{b} - 2\mathbf{h} = 0 \tag{58}$$

$$\mathbf{H} = \int \cdots \int \mathbf{x}\mathbf{x}^{\mathrm{T}}\,\mathrm{d}x_1 \cdots \mathrm{d}x_n, \quad \mathbf{h} = \int \cdots \int \mathbf{x} w\,\mathrm{d}x_1 \cdots \mathrm{d}x_n \tag{59}$$

$$\mathbf{b} = \mathbf{H}^{-1}\mathbf{h} \tag{60}$$

Appendix C. Approximate formula for linear natural frequency ω_1

In this paper, the actual linear mode has been adopted for spatial shape function of the pile, $\phi(\xi)$. This linear fundamental mode is obtained from a high order linear eigenvalue problem, see Section 3.1. In obtaining this eigenvector, the eigenvalue is also obtained and hence ω_1, see Fig. 2. However, for more than 4 generalised coordinates, it is not possible to obtain a closed form expression for this eigenvalue (root); Abel–Ruffini theorem. Thus, no simple and accurate closed form expression for ω_1 is obtainable using this approach.

In addition, a least square expression for $\omega_1(\alpha, \eta_1)$ was sought. However, no really good fit was easily achievable. So, as an alternate, an approximation of this linear mode shape was sought. It was obtained by applying a horizontal force at the pile head and using the pile deflected shape as an approximation to the linear mode. This approach only requires the inversion of the stiffness matrix **K** that is analytically obtainable in closed form for higher order systems. This was then used to obtain an closed form expression for $\omega_1(\alpha, \eta_1)$ using Eqs. (10) and (14); resulting in Eq. (61).

$$\omega_1 \simeq s\sqrt{\frac{s_n}{s_d}} \tag{61}$$

Formulae for s_n and s_d are given in Appendices C, D and E. Note that formula (61) is a very good engineering approximation. The correlation between (61) and Fig. 2 is high ($R^2 = 0.99$). Thus, it can be concluded, for this problem, that application of a point load at the lumped head mass produces an accurate estimate of the first mode across the entire space (α, η_1) likely to be encountered in practice.

Appendix D. Floating toe pile without cap formulae

$$\phi = \frac{q_n}{q_d} \tag{62}$$

$$\begin{aligned} q_n = {} & (1.855\mathrm{E}7\eta_1 - 2.172\mathrm{E}4\eta_1^2)\xi^6 - (4.174\mathrm{E}7\eta_1 - 8.26E4\eta_1^2)\xi^5 \cdots \\ & -1.125\mathrm{E}5\xi^4\eta_1^2 + (4.638\mathrm{E}7\eta_1 + 5.815\mathrm{E}4\eta_1^2)\xi^3 \cdots \\ & -(6.68\mathrm{E}9 + 3.403\mathrm{E}7\eta_1 + 8220\eta_1^2)\xi + (5.01\mathrm{E}9 + 1.18\mathrm{E}7\eta_1 + 1547\eta_1^2) \end{aligned} \tag{63}$$

$$q_d = 1547\eta_1^2 + 1.18\mathrm{E}7\eta_1 + 5.009\mathrm{E}9 \tag{64}$$

The functions, s_n and s_d, required to determine the linear frequency parameter $\omega_1$in equation (61) are given by (65) and (66), respectively.

$$s_n = \eta_1(1.534\mathrm{E}11\eta_1^4 + 5.273\mathrm{E}15\eta_1^3 + 3.783\mathrm{E}19\eta_1^2 + 1.951\mathrm{E}25 + 5.926\mathrm{E}22\eta_1) \tag{65}$$

$$\begin{aligned} s_d = {} & (3.35\mathrm{E}13\eta_1^4 + 5.112\mathrm{E}17\eta_1^3 + 2.167\mathrm{E}21\eta_1^2 + 1.655\mathrm{E}24\eta_1 + 3.512\mathrm{E}26)\alpha \cdots \\ & +2.335\mathrm{E}12\eta_1^4 + 4.233\mathrm{E}16\eta_1^3 + 2.629\mathrm{E}20\eta_1^2 + 2.556\mathrm{E}23\eta_1 + 9.106\mathrm{E}25 \end{aligned} \tag{66}$$

Appendix E. Floating toe pile with cap formulae

$$\phi = \frac{q_n}{q_d} \tag{67}$$

$$\begin{aligned} q_n = {} & (9.419\mathrm{E}6\eta_1^2 - 5822\eta_1^3)\xi^6 - (2.186\mathrm{E}8\eta_1 + 2.38\mathrm{E}7\eta_1^2 - 2.361\mathrm{E}4\eta_1^3)\xi^5 \cdots \\ & +(4.964\mathrm{E}6\eta_1^2 - 3.619\mathrm{E}4\eta_1^3)\xi^4 \cdots + (2.186\mathrm{E}9\eta_1 + 2.97\mathrm{E}7\eta_1^2 + 2.505\mathrm{E}4\eta_1^3)\xi^3 - (4.372\mathrm{E}9\eta_1 \\ & +2.222\mathrm{E}7\eta_1^2 + 6856\eta_1^3)\xi^2 \cdots + (2.624\mathrm{E}10 + 1.748\mathrm{E}9\eta_1 + 2.172\mathrm{E}6\eta_1^2 + 181\eta_1^3) \end{aligned} \tag{68}$$

$$q_d = 181\eta_1^3 + 2.173\mathrm{E}6\eta_1^2 + 1.747\mathrm{E}9\eta_1 + 2.624\mathrm{E}10 \tag{69}$$

The functions, s_n and s_d, required to determine the linear frequency parameter ω_1 in Eq. (61) are given by (70) and (71) respectively.

$$s_n = \eta_1(1.534\text{E}11\eta_1^4 + 5.273\text{E}15\eta_1^3 + 3.783\text{E}19\eta_1^2 + 1.951\text{E}25 + 5.926\text{E}22\eta_1) \tag{70}$$

$$\begin{aligned} s_d = {} & (3.35\text{E}13\eta_1^4 + 5.112\text{E}17\eta_1^3 + 2.167\text{E}21\eta_1^2 + 1.655\text{E}24\eta_1 + 3.512\text{E}26)\alpha \cdots \\ & + 2.335\text{E}12\eta_1^4 + 4.233\text{E}16\eta_1^3 + 2.629\text{E}20\eta_1^2 + 2.556\text{E}23\eta_1 + 9.106\text{E}25 \end{aligned} \tag{71}$$

References

[1] S. Bhattacharya, S. Adhikari, N.A. Alexander, A simplified method for unified buckling and dynamic analysis of pile supported structures in seismically liquefiable soils, *Soil Dynamics and Earthquake Engineering* 29 (2009) 1220–1235.
[2] R.L. Kondner, Hyperbolic stress–strain response: cohesive soils, *Journal of the Soil Mechanics and Foundations Division* 89 (1963) 115–144.
[3] Det Norske Veritas, Rules for the design, construction, and inspection of offshore structures, Appendix F; Foundations, Hovik, Norway, 1980.
[4] R.F. Scott, *Analysis of Centrifuge Pile Tests; Simulation of Pile Driving*, American Petroleum Institute, Washington, DC, USA, 1980.
[5] H. Matlock, Correlations for design of laterally loaded piles in soft clay, *Proceedings of the Second Annual Offshore Technology Conference*, Houston, USA, 1970.
[6] L.C. Reese, W.R. Cox, F.D. Koop, Analysis of laterally loaded piles in sand, *Proceedings of the Sixth Annual Offshore Technology Conference*, Houston, USA, 1974.
[7] J.M. Murchison, M.W. O'Neill, *Evaluation ofP–Y Relationships in Cohesionless Soils*, San Francisco, CA, USA, 1984, pp. 174–191.
[8] W. Finn, A study of piles during earthquakes: issues of design and analysis, *Bulletin of Earthquake Engineering* (2005) 141–234.
[9] J.M. Ting, C.R. Kauffman, M. Lovicsek, Centrifuge static and dynamic lateral pile behaviour, *Canadian Geotechnical Journal* 24 (1987) 198–207.
[10] J.M. Ting, Full-scale cyclic dynamic lateral pile responses, *Journal of Geotechnical Engineering* 113 (1987) 30–45.
[11] M.H. El Naggar, K.J. Bentley, Dynamic analysis for laterally loaded piles and dynamic *p–y* curves, *Canadian Geotechnical Journal* 37 (2000) 1166–1183.
[12] API, *Recommended Practice for Planning, Designing and Constructing Fixed Offshore Platforms—Working Stress Design—Includes Supplement 2*, American Petroleum Institute, 2000.
[13] J. Brinch Hansen, The Ultimate Resistance of Rigid Piles Against Transversal Forces, Danish Geotechnical Institute, Copenhagen, Denmark, Vol. 12, 1961, pp. 5–9.
[14] W.G.K. Fleming, A.J. Weltman, M.F. Randolph, W.K. Elson, *Piling Engineering*, Surrey University Press, London, 1992.
[15] L. Zhang, F. Silva, R. Grismala, Ultimate lateral resistance to piles in cohesionless soils, *Journal of Geotechnical and Geoenvironmental Engineering* 131 (2005) 78–83.
[16] M. Randolph, The challenges of offshore geotechnical engineering, *Ground Engineering* 38 (2005) 32–33.
[17] B.T. Kim, N.-K. Kim, W.J. Lee, Y.S. Kim, Experimental load-transfer curves of laterally loaded piles in Nak-Dong River sand, *Journal of Geotechnical and Geoenvironmental Engineering* 130 (2004) 416–425.
[18] *Dynamic Analysis and Earthquake Resistant Design, Strong Motion and Dynamic Properties*, vol. 1, Japanese Society of Civil Engineers, A.A. Balkema, Rotterdam, Brookfield, 1997.
[19] L. Verdure, J. Garnier, D. Levacher, Lateral cyclic loading of single piles in sand, *International Journal of Physical Modelling in Geotechnics* 3 (2003) 17–28.
[20] P.J. Holmes, D.A. Rand, Bifurcations of Duffings equation—application of catastrophe theory, *Journal of Sound and Vibration* 44 (1976) 237–253.
[21] Y. Ueda, Randomly transitional phenomena in the system governed by Duffings equation, *Journal of Statistical Physics* 20 (1979) 181–196.
[22] C. Pezeshki, E.H. Dowell, On chaos and fractal behavior in a generalized Duffings system, *Physica D* 32 (1988) 194–209.
[23] F.N.H. Robinson, Experimental-observation of the large-amplitude solutions of Duffings and related equations, *IMA Journal of Applied Mathematics* 42 (1989) 177–201.
[24] L.C. Reese, H. Matlock, Non-dimensional solutions for laterally loaded piles with soil modulus assumed proportional tp depth, *Proceedings of the Eighth Texas Conference on Soil Mechanics and Foundation Engineering*, Austin, TX, 1956, pp. 1–41.
[25] G. Rega, A.H. Nayfeh, *Nonlinear Interactions: Analytical, Computational, and Experimental Methods*, Wiley Series in Nonlinear Science, Vol. 760, Wiley, New York, 2000 (*Meccanica*, 35 (2000) 583–586).
[26] E. Gourdon, N.A. Alexander, C.A. Taylor, C.H. Lamarque, S. Pernot, Nonlinear energy pumping under transient forcing with strongly nonlinear coupling: theoretical and experimental results, *Journal of Sound and Vibration* 300 (2007) 522–551.
[27] E.J. Doedel, A.R. Champneys, T.F. Fairgrieve, Y.A. Kuznetsov, B. Sandstede, X. Wang, AUTO 97: Continuation and Bifurcation Software for Ordinary Differential Equations (with HomCont), Technical Report, Concordia University, 1997.
[28] N.A. Alexander, F. Schilder, Exploring the performance of a nonlinear tuned mass damper, *Journal of Sound and Vibration* 319 (2009) 445–462.
[29] A.H. Nayfeh, N.E. Sanchez, Bifurcations in a forced softening Duffing oscillator, *International Journal of Non-Linear Mechanics* 24 (1989) 483–497.
[30] L.N. Virgin, L.A. Cartee, A note on the escape from a potential well, *International Journal of Non-Linear Mechanics* 26 (1991) 449–452.
[31] K. Yagasaki, Detection of bifurcation structures by higher-order averaging for Duffing's equation, *Nonlinear Dynamics* 18 (1999) 129–158.
[32] C. Hayashi, *Non-linear Oscillations in Physical Systems*, McGraw-Hill, New York, 1964.
[33] *MATLAB* (*the language of technical computing*), seventh ed., The Mathworks Inc., 2005.
[34] T. Koskusho, *Dynamic Deformation Properties of Soil and Nonlinear Seismic Response*, Vol. 301, Central Research Institute of Electric Power Industry, Japan, 1982.
[35] K. Nishi, Y. Yoshida, Y. Sawada, T. Iwadate, T. Kokusyo, Soil-structure interaction of JPDR reactor, 2. Static and dynamic mechanical properties of sand and sandy gravel by laboratory tests and proposal of model of ground, *Denryoku Chuo Kenkyusho Hokoku (Japan)* 383002 (1983) 1–44.
[36] B.O. Hardin, V.P. Drnevich, Shear modulus and damping in soils: measurement and parameter effects, *American Society of Civil Engineers, Journal of the Soil Mechanics and Foundations Division* 98 (1972) 603–624.
[37] M.L. Silver, H.B. Seed, Deformation characteristics of sands under cyclic loading, *Journal of the Soil Mechanics and Foundations Division* 97 (1971) 1081–1098.
[38] N.A. Alexander, Evaluating basins of attraction in non-linear dynamical systems using an improved recursive boundary enhancement (RBE), *Journal of Sound and Vibration* 209 (1998) 443–447.
[39] N.A. Alexander, Evaluating the global characteristic of a nonlinear dynamical system with recursive boundary enhancement, *Advances in Engineering Software* 29 (1998) 707–716.
[40] J.M.T. Thompson, S.R. Bishop, L.M. Leung, Fractal basins and chaotic bifurcations prior to escape from a potential well, *Physics Letters A* 121 (1987) 116–120.
[41] F.E. Richart, J.R. Hall, R.D. Woods, *Vibrations of Soils and Foundations*, Prentice-Hall, Inc., 1970.
[42] S. Adhikari, S. Bhattacharya, Dynamic instability of pile-supported structures in liquefiable soils during earthquakes, *Journal of Shock and Vibration*, 2008.
[43] S. Bhattacharya, A. Blackborough, S.R. Dash, Collapse of piled-foundations in liquefiable soils-an example of design-based error, *Proceedings of the Institution of Civil Engineers*, Civil Engineering, UK, 2008.

[44] S. Bhattacharya, S.R. Dash, S. Adhikari, On the mechanics of failure of pile-supported structures in liquefiable deposits during earthquakes, *Current Science* 94 (2008) 605–611.
[45] S. Bhattacharya, S.P.G. Madabhushi, M.D. Bolton, An alternative mechanism of pile failure in liquefiable deposits during earthquakes, *Geotechnique* 54 (2004) 203–213.
[46] K.M. Rollins, K.T. Peterson, T.J. Weaver, Lateral load behavior of full-scale pile group in clay, *Journal of Geotechnical and Geoenvironmental Engineering* 124 (1998) 468–478.
[47] K.M. Rollins, J.D. Lane, T.M. Gerber, Measured and computed lateral response of a pile group in sand, *Journal of Geotechnical and Geoenvironmental Engineering* 131 (2005) 103–114.
[48] J.F. Stanton, S. Banerjee, I. Hasayen, Shaking table tests on piles, University of Washington, USA, 1988.
[49] A. Boominathan, R. Ayothiraman, Dynamic behaviour of laterally loaded model piles in clay, *Proceedings of the Institution of Civil Engineers: Geotechnical Engineering* 158 (2005) 207–215.